JOURNAL OF MATERIALS SCIENCE 25 (1990) 4066–4074

The effect of eccentricity on dynamic crack propagation behaviour of rubber-modified PMMA models

G. A. PAPADOPOULOS
Department of Engineering Science, Section of Mechanics, The National Technical University of Athens, 5, Heroes of Polytechnion Avenue, GR-15773 Athens, Greece

G. C. PAPANICOLAOU
Department of Mechanical Engineering, Section of Mechanics, University of Patras, GR-26110 Patras, Greece

Rubber-modified materials show a complex fracture behaviour. In a previous paper the influence of a rigid PMMA circular inclusion with a rubber ring surrounding it embedded in a PMMA matrix, on the dynamic fracture mode was investigated. In the present experimental study, the same model system was used to investigate the effect of eccentricity of the initial crack path from the specimen centreline on which the complex inclusion centre is located, on the dynamic crack propagation mode. This effect was studied by using high-speed photography and dynamic caustics. It was shown that the eccentricity of the initial crack path largely determines both the crack propagation delay observed as the crack approaches the complex inclusion and the bifurcation of the crack. It was also found that the maximum crack propagation velocity, the length of the crack path along the interface, as well as the angle of incidence with which the propagating crack meets the interface, increase as the eccentricity increases.

1. Introduction

It is well known that brittle polymers can be toughened by the addition of small amounts of rubber particles [1, 2]. The most common technique usually followed for the production of rubber-modified plastics is to resolve rubber as a separate phase which may incorporate inclusions of the polymer. Recently, some attempts have been made to toughen thermoplastics by blending with recycled rubber crumb [3–5].

There are several types of rubber-particle structure. Among them the most common are the "core shell' and "onion" structure. In the former type, each polymer inclusion is surrounded by a concentric thin spherical shell of rubber, while in the "onion" structure there are several concentric spheres of rubber and polymer [6–9].

The role of toughening mechanisms encountered in rubber-modified plastics is to dissipate strain energy that would otherwise be available to extend an existing flow or crack. Toughening mechanisms include shear yielding and crazing, interaction between them and finally diversion and multiplication of a growing crack. Because the rubber is incompressible, having a Poisson's ratio of about 0.5, a dilatational stress field is developed at the plastic–rubber interface as a result of which the development of crazing is encouraged. Crazing is developed in a direction perpendicular to that of the applied stress and initiated at the rubber–matrix interface. The smaller the interparticle distance, the higher are the craze density and thus the higher the ultimate fracture energy.

The structure of crazes is distinct from that of the bulk polymer: the bulk is porous, with a void content of about 40% [10] and the polymer chains are partially aligned parallel to the load [11, 12]. As the crazes are weaker than the bulk they provide sites for the initiation of fracture. Crack propagation occurs by the continued formations and rupture of crazed material.

However, crazing is not the only toughening mechanism encountered in rubber-modified polymers. Various theories have been proposed to explain fracture toughness of two-phase polymers. Observations of stress-whitening and density decreases on straining in hot isostatically pressed sytrene (HIPS) led Merz *et al.* [13] to the suggestion that many small cracks were formed on straining, but the rubber particles spanned the cracks and hindered further crack growth. The same authors showed that optimum toughness corresponds to a specific size of the rubber domains existing in the material. An alternate energy-absorption mechanism has been proposed [14], according to which rubber particles act as stress concentrators so that many microcracks are developed around them. Also, it was postulated that rubber particles act as crack stoppers while due to their ability to absorb a great deal of energy when stretched, higher fracture

0022–2461/90 $03.00 + .12

energies are required. Next, according to the theory developed by Newman and Strella [15], rubber influence of which the T_g of the matrix material is lowered sufficiently to permit facile cold-drawing and shear yielding.

Another important factor which determines the fracture toughness of rubber-modified polymers is the rubber particle size. Various theories have been concerned with particle size. However, some of them indicate an increase in toughness with a respective increase in particle size [16, 17] while other studies suggest an increase in toughness with a decrease in particle size [17, 18]. Each of these cases is understandable using the model described by Sudduth [19]. According to this model there is a maximum probable impact strength at a specific particle size that depends on the graft level required to achieve compatibility between the two phases. Particle size may affect fracture in another way. More specifically, during the crack propagation process, a plastic zone is developed at the tip of the crack the size of which depends on the type of the material. If the particle size is small compared to the size of the plastic zone, the particle size does not affect the continuum aspects of the fracture process. However, because the size of the plastic zone is changed during the crack propagation process, there is an overall effect of the particles on the relaxation spectrum of the material. The effect of the particles on the time-dependence response characteristics is more pronounced when particles are large compared to the size of the plastic zone developed at the tip of the crack, because in that case there is a strong stress interaction between the tip of the advancing crack and the filler particles.

In addition, the nature of the interfacial bond between matrix and particles is of crucial importance. In fact, perfect adhesion corresponding to continuity of stresses and displacements at the interface is a most common assumption for analytical treatments. However, with real composites, this condition is very seldom fulfilled. The morphology of rubber-modified polymers is expected to be quite complex. Rubber–matrix interfaces and/or interphases may be involved [19]. Also, as is well known, in the region between matrix and filler a third phase is developed consisting of areas of imperfect adhesion, stress concentrations, microcracks, impurities and other defects [20–28]. The microcracks developed in this third phase are centres from which failure almost always begins. The rate of crack growth depends strongly on the degree of inhomogeneity of the material not only in the macroscopic sense of the term, but rather on its microscopic sense. This means that if we consider the composite as being macroscopically homogeneous, the factor upon which the rate of the crack growth depends is the microscopic inhomogeneity which characterizes the region surrounding the particles. A strong interface can first submit the applied stress to the matrix and enhance crazing and then help share the stress with the matrix after crazing; a weak interface would tend to permit easy cavitation at the interface rather than crazing in the matrix, and would be expected to lower the fracture energy. In addition, an ill-defined boundary may serve to blunt or slow down growing cracks more effectively; in general, the fracture path tends to proceed through the interfacial region.

An impedance mismatch, i.e. when $\rho_2 c_2 \gg \rho_1 c_1$ (c is the velocity of propagation of stress waves), which is common in rubber-modified polymers, tends to create a situation, similar to those caused by imperfect bonding. Indeed, a stress wave practically does not enter the reinforcing particle, but simply circumvents it. The particle in this case only perturbs the stress field by restraining the matrix, provided that the strain is sufficiently high.

Another important role of rubber particles is to initiate branches in very fast cracks. This is because when the crack speed is greater than about one-half the speed of sound in the material under consideration the crack is unable to dissipate enough energy to remain stable so that it tends to split into several branches.

The effect of rubber-particle content and loading rate on the crack propagation mode has been studied [29]. Also, the influence of a rigid PMMA circular inclusions with a rubber ring surrounding it, "complex inclusion" embedded in a PMMA matrix, on the dynamic fracture mode was investigated [30].

In the present study the influence of a "complex" inclusion and the effect of eccentricity of the initial crack path on the dynamic crack propagation mode was studied. The results of crack propagation mode observation, fracture toughness and crack propagation velocity measurements are presented here.

2. The experimental method of dynamic caustics

The experimental method of dynamic caustics was applied for the study of the influence of inclusions to the crack propagations path [31, 32].

A convergent or divergent light beam impinges on the specimen in the close vicinity of the crack tip and the transmitted rays are received on a reference plane, parallel to the plane of the specimen. These rays are scattered and are concentrated along a strongly illuminated curve on the reference plane placed at a distance

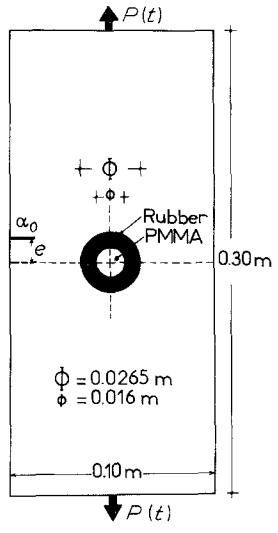

Figure 1 Geometry of specimen. a_0 = 0.010 m and e = 0, 0.0025, 0.005, 0.0075, 0.010, 0.0125 and 0.015 m.

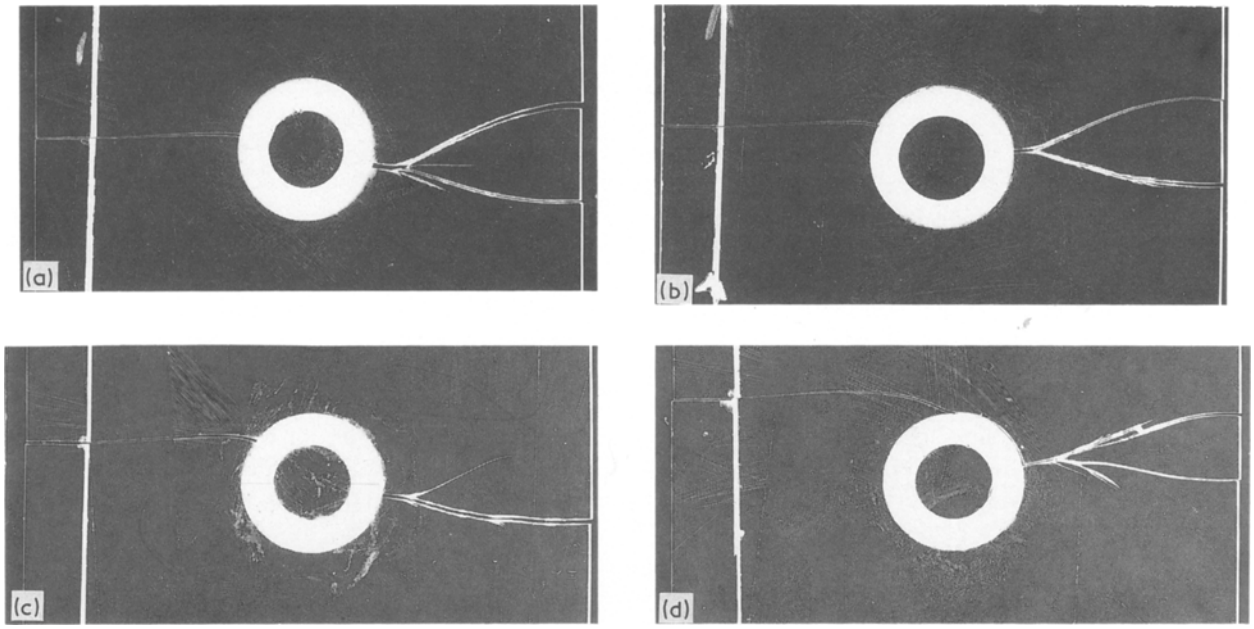

Figure 2 Photographs showing crack propagation in specimens having one "complex" inclusion with a rubber interphase. The eccentricities were (a) $e = 0.0025\,\text{m}$, (b) $e = 0.005\,\text{m}$, (c) $e = 0.0075\,\text{m}$ and (d) $e = 0.015\,\text{m}$. The strain-rate was $\dot{\varepsilon} = 4\,\text{sec}^{-1}$.

z_0 from the specimen, which is called "caustic" [33, 34]. From the size and the angular displacement, ϕ, of the axis of symmetry of the caustic relative to the crack axis, it is possible to calculate the stress intensity factors, K_I^d and K_{II}^d, for the case of mixed-mode conditions by the relations

$$K_I^d = \frac{2(2\pi)^{1/2}}{3z_0 d\lambda_m^{3/2} c_t}\left[\frac{D_t^{max}}{\delta_t^{max}(v)}\right]^{5/2} \quad (1)$$

$$K_{II}^d = K_I^d \tan\frac{\phi}{2} \quad (2)$$

where c_t is the optical constant of the material, d is the thickness of the specimen, λ_m is the magnification ratio of the optical set-up, z_0 is the distance between specimen and reference plane, D_t^{max} is the maximum transverse diameter of the caustic and $\delta_t^{max}(v)$ is a correction factor which depends on the crack velocity. This correction factor is given by nomograms in [31].

3. Experimental procedure

The matrix material chosen for the present experimental investigation was in all cases PMMA. The specimens used were in the form of rectangular plates with dimensions $0.30 \times 0.10 \times 0.003\,\text{m}^3$ with an edge artificial crack of length $a_0 = 0.010\,\text{m}$. The eccentricity of the initial crack path from the specimen centreline on which the "complex" inclusion centre was $e = 0$, 0.0025, 0.0050, 0.0075, 0.010, 0.0125 and 0.0150 m. The inclusion diameter was 0.016 m, whereas the outer diameter of the rubber ring was 0.0265 m (Fig. 1).

The specimens were subjected to a dynamic tensile load until fracture by a Hydropulse High-speed Testing machine (Carl-Shenk Co.) with a maximum possible strain rate $\dot{\varepsilon} = 80\,\text{sec}^{-1}$. For the recording of the dynamic-crack propagation, a Cranz-Scharding high-speed camera was used disposing 24 sparks with a maximum frequence of 10^6 frames sec^{-1}. In the optical set-up used in the experiments the following quantities were taken: $z_0 = 0.80\,\text{m}$, $\lambda_m = 0.75$. The dynamic properties of PMMA are $E = 4.3 \times 10^9\,\text{N m}^{-2}$, Poisson's ratio $\nu = 0.34$ and stress optical constant $c_t = 0.74 \times 10^{-10}\,\text{m}^2\,\text{N}^{-1}$ [31]. The loading rate applied in the present work was $\dot{\varepsilon} = 4\,\text{sec}^{-1}$.

4. Results and discussion

In order to study the influence of interfacial adhesion and the effect of eccentricity on the crack propagation path, a number of specimens in the form shown in Fig. 1 was used. In all cases the specimens had an edge transverse artificial crack of length $a_0 = 0.010\,\text{m}$ while the eccentricity of the initial crack with respect to the centreline was varied. The dynamic crack propagation of rubber-modified composite models similar to that mentioned above with central initial cracks, has been studied previously [30].

Fig. 2 shows typical crack paths of four specimens fractures under strain rate $\dot{\varepsilon} = 4\,\text{sec}^{-1}$. The respective eccentricity values were as follows: (a) $e = 0.0025\,\text{m}$,

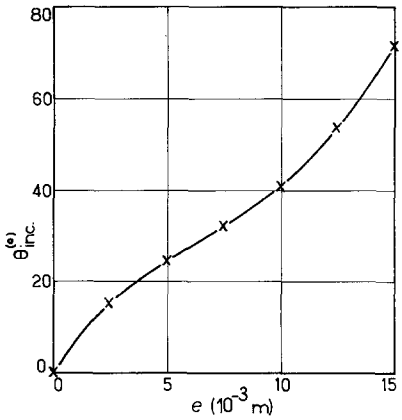

Figure 3 Variation of the incidence angle, $\theta_{inc.}$, at the interface of the inclusion, of the propagating crack with the eccentricity, e, of the initial crack.

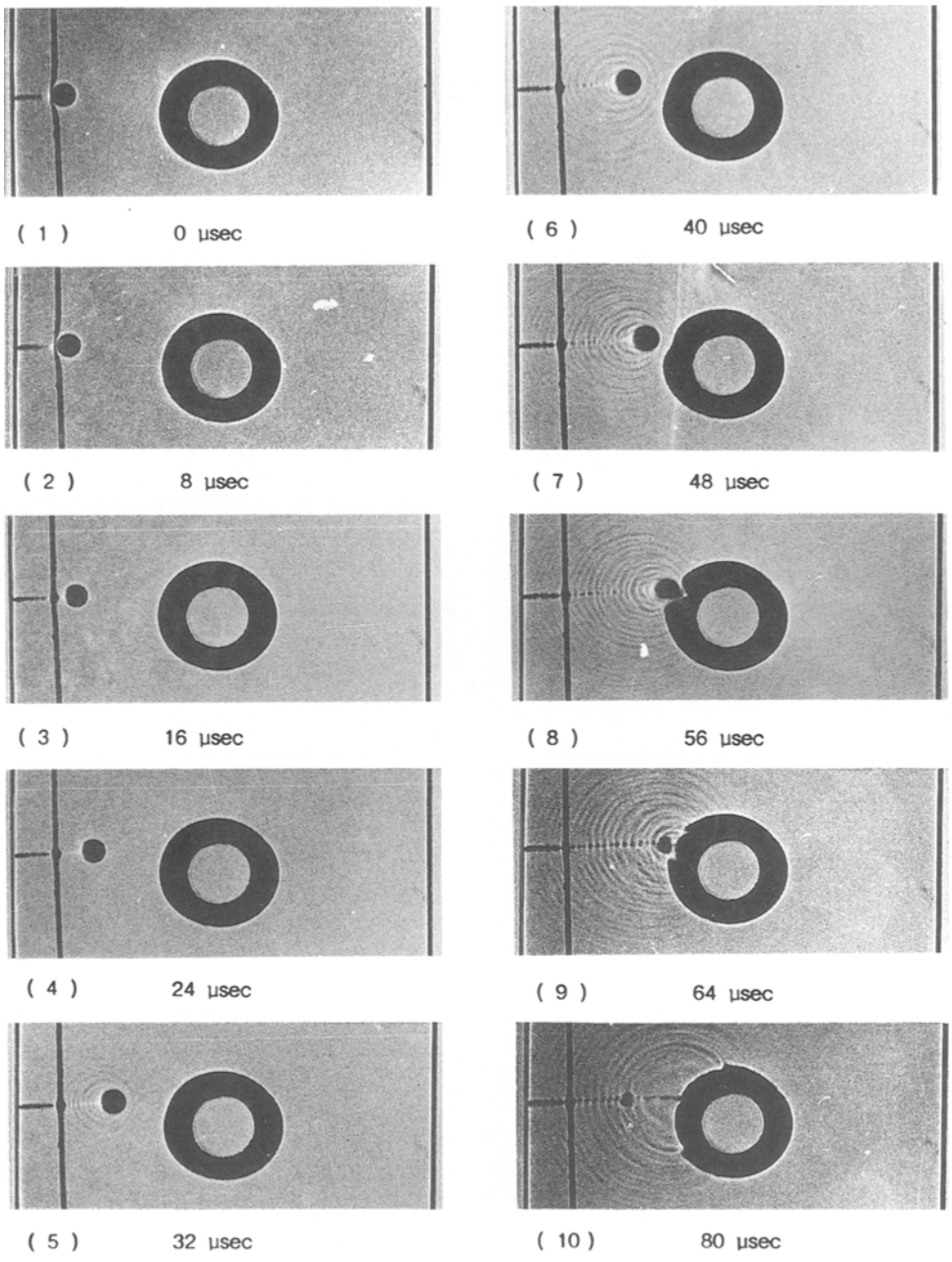

Figure 4 A series of photographs showing the crack propagation in a specimen having one "complex" inclusion. The eccentricity of the initial crack was $e = 0$ m and the strain rate was $\dot{\varepsilon} = 4\,\text{sec}^{-1}$.

(b) $e = 0.0050$ m, (c) $e = 0.0075$ m and (d) $e = 0.0150$ m. From these photographs it may be observed that: (i) as the crack approaches the complex inclusion, it splits into two branches, each one of them following the rubber–matrix interface thus forming an interface path. The lengths of the two interface crack paths have a ratio which is inversely proportional to the eccentricity; (ii) the incident crack on the interface makes an angle θ_{inc} with the radius of the inclusion at the point of incidence which increases with the eccentricity of the initial crack. The variation of this angle with respect to the eccentricity is shown in Fig. 3. The observed inclination of the incident crack with respect to the normal at the inclusion surface at the point of incidence may be due to the interaction of the stress fields around the crack and the inclusion; (iii) as the two interface crack branches surpass the

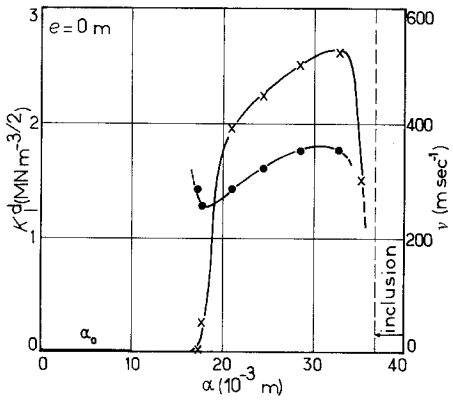

Figure 5 Variation of the stress intensity factor K_I^d (●) and the crack propagation velocity, v (x) with the crack length, a, for a specimen with an eccentricity of the initial crack $e = 0$ m and for strain rate $\dot{\varepsilon} = 4\,\text{sec}^{-1}$.

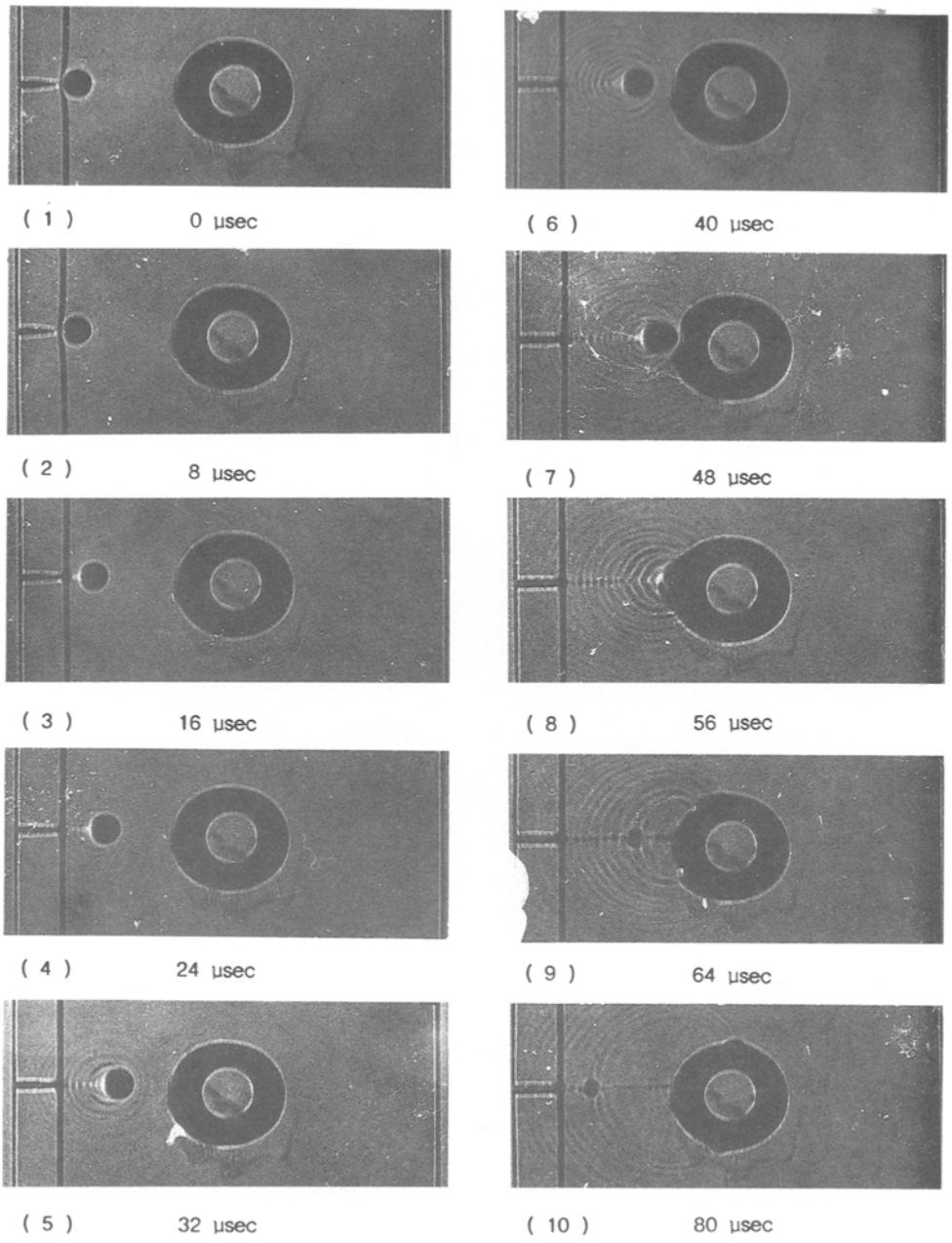

Figure 6 As Fig. 4 for eccentricity $e = 0.0025$ m.

circumference of the inclusion they meet each other at another point on the interface, which is not antidiametrical to the point of incidence, from which a unique crack emerges which immediately bifurcates independently of the eccentricity value; (iv) there is always an "attraction" of the crack from the inclusion area.

The detailed crack propagation process may be studied from the series of photographs taken with a Cranz-Schardin high-speed camera. Fig. 4 presents a series of photographs showing the crack propagation process in the case of a single complex inclusion and with eccentricity value $e = 0$. From these photographs we may see that as the crack tip approaches the complex inclusion an intense deformation of the rubber interphase is observed (Fig. 4, frames 5 to 7). A part of the energy delivered is absorbed by the rubber while the rest is consumed by the reflected stress waves (Fig. 4, frames 8 and 9). At the same time, the end points of the reflected stress fronts follow symmetrically the rubber–matrix interface and thus forming an interface crack path. After a period of time (arrest time) an amount of energy is concentrated at the antidiametrical point and the crack starts propagating again in the matrix material. The crack arrest time in the present case was more than 50 μsec depending on the nature and quality of the bond that

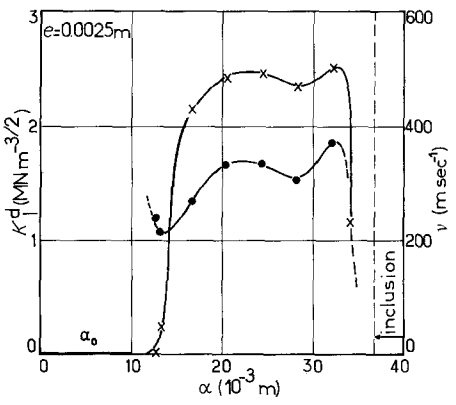

Figure 7 As Fig. 5 for eccentricity $e = 0.0025$ m.

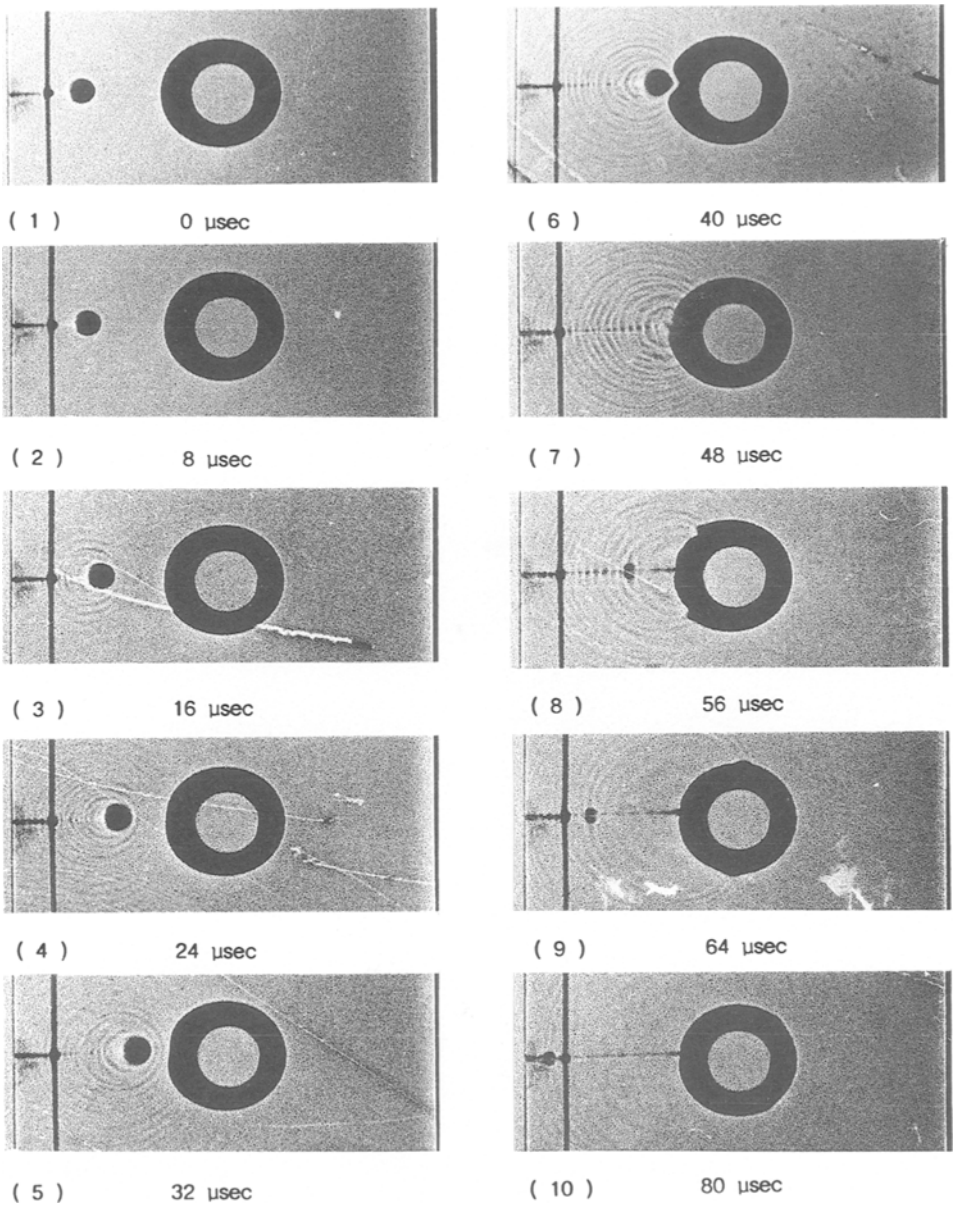

Figure 8 As Fig. 4 for eccentricity $e = 0.005$ m.

exists between rubber and matrix. As the crack propagates, its tip acts as a centre for spherical stress wavelets. These waves are transverse shear waves and in the case of PMMA have a speed of $c_2 = 1200$ m sec^{-1} [19]. Also in Fig. 4 (frames 8 and 9) an elastic deformation having the form of a faint caustic is observed which propagates backwards along the crack tips direction with a speed of 1150 m sec^{-1}. This value almost coincides with the respective value of the speed c_2 of the transverse waves. From this fact we may conclude that when the crack tip arrives at the rubber–matrix interface a transverse wave is developed which, in turn, is reflected by the interface and then moves backwards. The centre of this wave is the faint caustic observed on these photographs. The wavefronts of this wave are responsible for the observed elastic deformation of the rubber ring (Fig. 4, frames 8 and 9). The time needed for the crack to approach the interface is about 48 μsec.

The variation of stress intensity factor, K_I^d, and the crack propagation velocity v, as a function of the crack length, a, for the specimen shown in Fig. 4 is given in Fig. 5. From this figure it may be observed that when the crack tip approaches the inclusion both K_I^d and v attain a maximum value and subsequently afterwards an abrupt decrease is observed. Next, the main crack stops momentarily while the interface crack propagates around the inclusion. During this time there is no principal crack propagation effect and

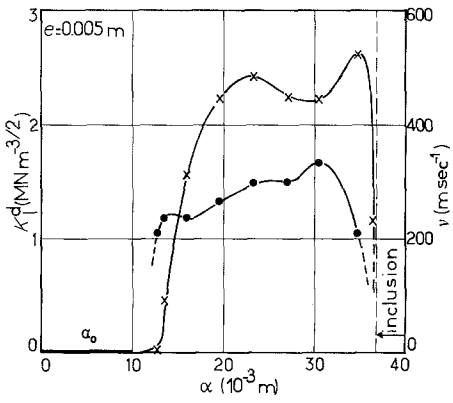

Figure 9 As Fig. 5 for eccentricity $e = 0.005$ m.

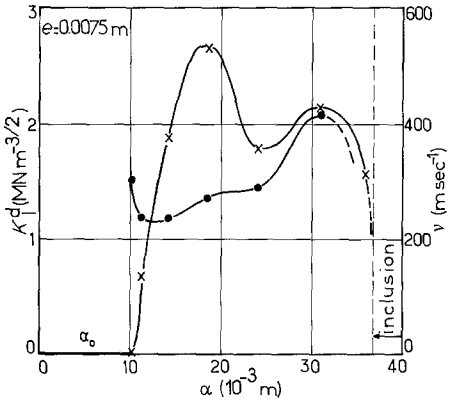

Figure 10 As Fig. 5 for eccentricity $e = 0.0075$ m.

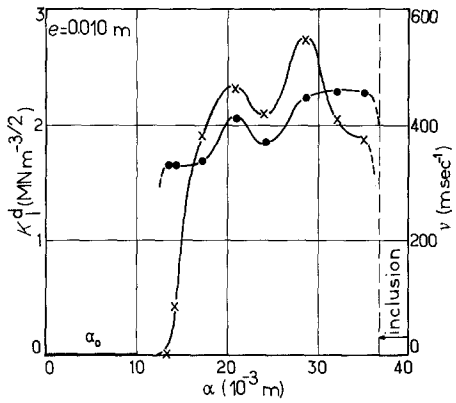

Figure 11 As Fig. 5 for eccentricity $e = 0.010$ m.

a crack arrest is achieved. A great part of the energy is absorbed by the rubber interphase and there is no energy transmission to the PMMA inclusion. Thus the role of the rubber interphase is to protect the main inclusion from the effect of the stress waves developed due to the crack propagation process. The degree of this protection depends on the quality of adhesion and the degree of compatibility of the constituent materials. Similar phenomena are also observed in the case where the eccentricity, e, of the initial crack takes values different to $e = 0$.

Fig. 6 presents a series of photographs showing

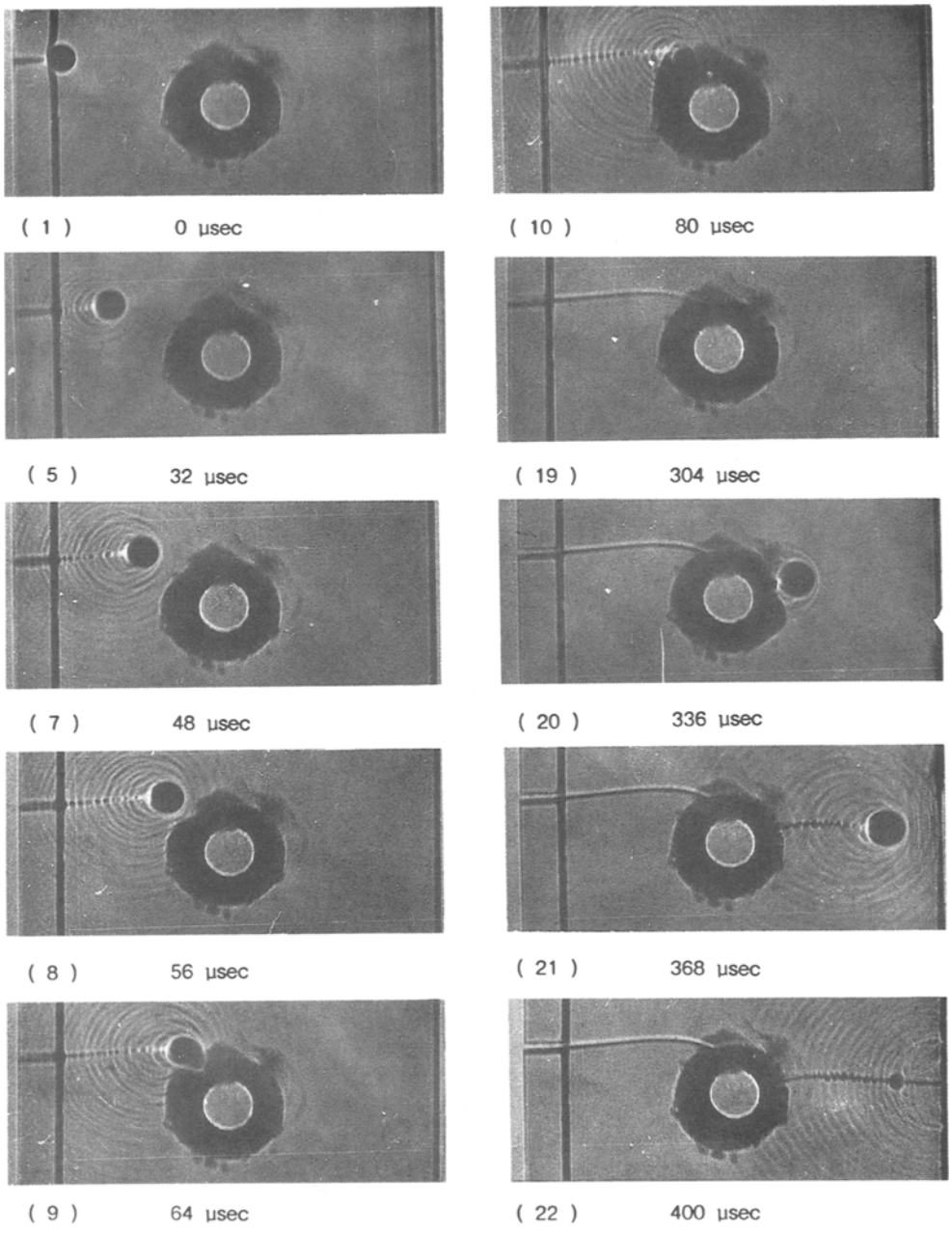

Figure 12 As Fig. 4 for eccentricity $e = 0.0125$ m.

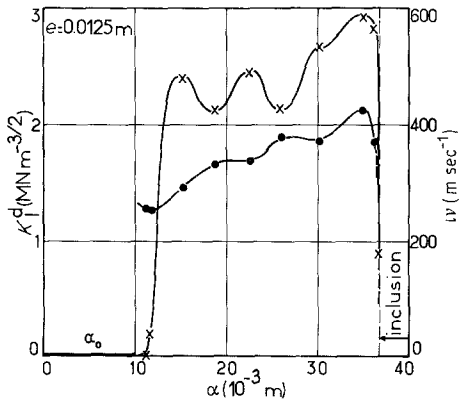

Figure 13 As Fig. 5 for eccentricity $e = 0.0125$ m.

the crack propagation in a specimen having one "complex"inclusion. The eccentricity of the initial crack was $e = 0.0025$ m and the strain rate was $\dot{\varepsilon} = 4\,\text{sec}^{-1}$. From these photographs we may observe the same phenomena as observed in Fig. 4. The time needed for the crack to approach the inclusion is about 56 μ sec, i.e. greater than the respective time in the case where $e = 0$.

The variation of the stress intensity factor, K_I^d, and the crack propagation velocity, v, with the crack length, a, for the specimen shown in Fig. 6 is given in Fig. 7. It may be observed that when the crack tip approaches the inclusion, both v and K_I^d attain a maximum value and subsequently afterwards an abrupt decrease is observed. Next, the main crack stops momentarily while the interface crack propagates around the inclusion.

Fig. 8 presents a series of photographs showing the crack propagation in a specimen with one "complex" inclusion. The eccentricity of the initial crack was $e = 0.005$ m and the strain rate $\dot{\varepsilon} = 4\,\text{sec}^{-1}$. As the crack tip approaches the inclusion the same intense phenomena are observed as in previous cases. The time needed for the crack to approach the inclusion is about 64 μsec. We may also observe the initiation and propagation of the stress waves originated from the tip of the crack (frames 8 to 10).

Fig. 9 shows the variation of the stress intensity factor K_I^d, as well as that of crack propagation velocity, v, as a function of crack length, a. We may observe that when the crack tip is in the close vicinity of the "complex" inclusion interface, v attains a maximum value of about 521 m sec^{-1} and subsequently

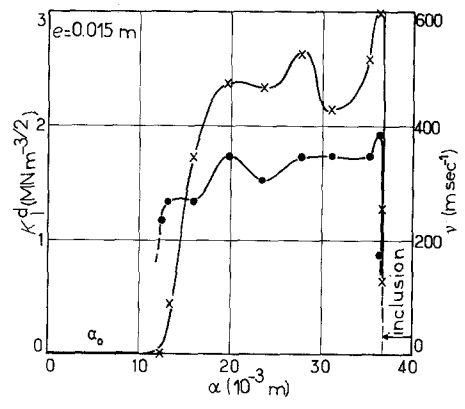

Figure 14 As Fig. 5 for eccentricity $e = 0.015$ m.

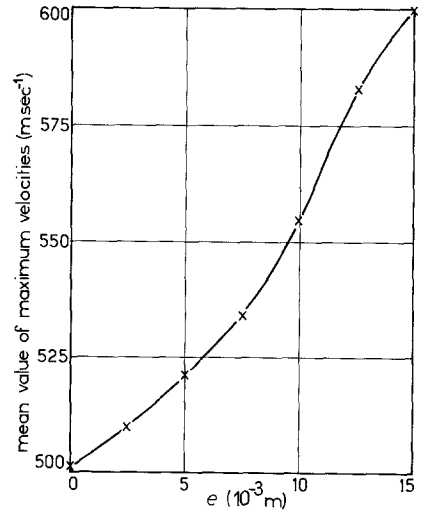

Figure 15 Variation of the maximum velocity of the propagating crack with the eccentricity, e, of the initial crack.

dramatically decreases to diminish when the crack tip arrives at the interface of the inclusion. The maximum value for K_I^d is attained earlier than the respective maximum for the crack propagation velocity. The variation of K_I^d as well as of v as a function of crack length, a, for the cases where the eccentricity has values $e = 0.0075$ and 0.010 m is shown in Figs 10 and 11, respectively.

Fig. 12 presents a series of photographs showing the crack propagation process in a specimen with eccentricity of the initial crack $e = 0.0125$ m. The applied strain rate was $\dot{\varepsilon} = 4\,\text{sec}^{-1}$. We may observe the way that the crack approaches the inclusion. The measured time for the crack to approach the inclusion was about 80 μsec. Next, we may observe that the point of initiation of the final crack is very close to the point of incidence of the initial main crack on the circumference of the inclusion. The variation of K_I^d as well as of v as a function of crack length, a, for the specimen in Fig. 12 is shown in Fig. 13. The maximum values of v and K_I^d attained in the close vicinity of the "complex" inclusion, are 580 m sec^{-1} and 1.89 MN m$^{3/2}$, respectively. The measured crack arrest time was about 256 μsec and subsequently after this arrest time a new crack propagates. The final crack is characterized by higher values of velocity and K_I^d in comparison with the respective values of the initial crack.

When the eccentricity, e, is 0.015 m, we may observe from Fig. 14 that $v_{max} \simeq 600\,\text{m sec}^{-1}$ while $K_{I(max)}^d$ remains unchanged when compared to the previous experiments.

Fig. 15 shows the variation of v_{max} as a function of

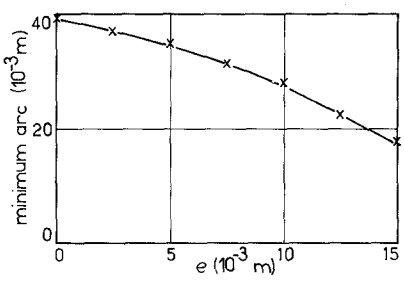

Figure 16 Variation of the minimum propagating arc around the "complex" inclusion with the eccentricity, e, of the initial crack.

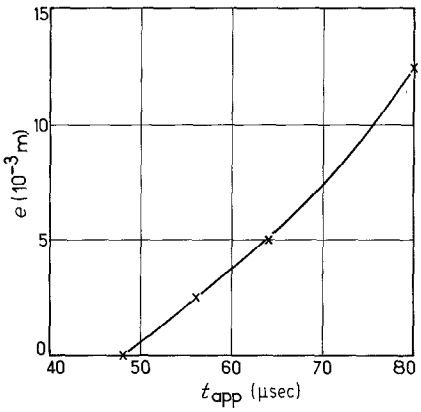

Figure 17 Variation of the approaching time, $t_{app.}$, of the initial crack to the inclusion interface with the eccentricity, e, of the initial crack.

eccentricity, e. We may observe that v_{max} increases with e. Another important observation is that the interface crack length measured from the side of the initial eccentricity decreases as the eccentricity increases. This variation is shown in Fig. 16. The point of initiation of the final crack greatly depends on the interface crack length.

Finally, the time required for the initial crack to approach the inclusion, t_{app}, increases with the eccentricity, e, and this is shown in Fig. 17.

5. Conclusion

In the present work the effect of eccentricity of the initial edge crack on the dynamic crack propagation of several rubber-modified composite models has been studied. The results may be summarized as follows.

1. In all cases the crack propagation velocity, v, as well as K_I^d attain a maximum value when the crack tip is in the close vicinity and in front of the inclusion. This is followed by an abrupt decrease of the respective v and K_I^d values.

2. In all cases as the crack tip approaches the inclusion an intense deformation of the rubber interphase and an interface crack path were observed. These effects were accompanied by a crack delay or a crack arrest time which was of the order of 256 μsec.

3. The velocity, v_{max}, increases with the eccentricity.

4. The interface crack path decreases as the eccentricity increases.

5. The existence of the "complex" inclusion "attracts" the crack which in turn falls on to the interface in a direction not normal to the inclusion and this was attributed to stress-field interaction.

References

1. C. B. BUCKNALL, "Toughened Plastics" (Applied Science, London, 1977).
2. S. NEWMAN, in "Polymer Blends", Vol. 2, edited by D. R. Paul and S. Newman (Academic, New York, 1978) Ch. 13.
3. R. P. BURFORD and M. PITTOLO, *J. Mater. Sci.* **21** (1986) 2308.
4. M. PITTOLO and R. P. BUFORD, *ibid.* **21** (1986) 1769.
5. *Idem, Rubber Chem. Technol.* **58** (1985) 97.
6. G. RIES, M. SCHLIENGER and S. MARTIN, *J. Macromol. Sci. (Phys.)* **B17** (1980) 355.
7. A. ECHTER, *Angew. Macromol. Chem.* **58/59** (1977) 175.
8. C. B. BUCKNALL, F. F. P. COTE and I. K. PARTRIDGE, *J. Mater. Sci.* **21** (1986) 301.
9. C. B. BUCKNALL, P. DAVIES and I. K. PARTRIDGE, *ibid.* **21** (1986) 307.
10. R. P. KAMBOUR, *J. Polym. Sci.* **A2** (1964) 4159.
11. O. K. SPURR and W. D. NIEGISH, *J. Appl. Poly. Sci.* **6** (1962) 585.
12. D. G. GRAND, R. P. KAMBOUR and W. F. HAAF, *J. Polym. Sci. A-2* **10** (1972) 1565.
13. E. H. MERZ, G. C. CLAVER and M. BAIRR, *ibid.* **22** (1956) 325.
14. J. A. SCHMITT and H. KESKKULA, *J. Appl. Polym. Sci.* **3** (1960) 132.
15. S. NEWMAN and S. STRELLA, *ibid.* **9** (1965) 2297.
16. K. DINGES and H. SCHUSTER, *Makromol. Chem.* **101** (1967) 200.
17. R. P. KAMBOUR. *J. Polym. Sci. Macromol. Rev.* **7** (1973) 112.
18. C. F. PARSONS and E. L. SUK, *Chem. Ser.* **99** (1971).
19. R. D. SUDDUTH, *J. Appl. Polym. Sci.* **99** (1978) 2427.
20. G. C. PAPANICOLAOU, S. A. PAIPETIS and P. S. THEOCARIS, *Colloid Polym. Sci.* **256** (1978) 689.
21. G. C. PAPANICOLAOU and P. S. THEOCARIS, *ibid.* **257** (1979) 239.
22. P. S. THEOCARIS and G. C. PAPANICOLAOU, *Fibre Sci. Technol.* **12** (1979) 421.
23. G. C. PAPANICOLAOU, P. S. THEOCARIS and G. D. SPATHIS, *Colloid. Polym. Sci.* **258** (1980) 1231.
24. P. S. THEOCARIS, G. C. PAPANICOLAOU and G. D. SPATHIS, *Fibre. Sci. Technol.* **15** (1981) 187.
25. P. S. THEOCARIS, E. P. SIDERIDIS and G. C. PAPANICOLAOU, *J. Reinforced Plastics and Composites* **4** (1985) 396.
26. E. P. SIDERIDIS, P. S. THEOCARIS and G. C. PAPANICOLAOU, *Rheologica Acta* **25** (1986) 350.
27. C. D. PAPASPYRIDES, G. C. PAPANICOLAOU and T. DUVIS, *Mater. Chem. Phys.* **17** (1987) 531.
28. G. C. PAPANICOLAOU and C. D. PAPASPYRIDIS, *ibid.* **17** (1987) 453.
29. J. MILIOS, G. C. PAPANICOLAOU and R. J. YOUNG, *J. Mater. Sci.* **21** (1986) 4281.
30. G. A. PAPADOPOULOS and G. C. PAPANICOLAOU, *ibid.* **23** (1988) 3421.
31. P. S. THEOCARIS and G. A. PAPADOPOULOS, *Engng Fract. Mech.* **13** (1980) 683.
32. *Idem,* ASTM STP 971 (American Society for Testing and Materials, Philadelphia, Pennsylvania, 1983) II-320.
33. P. S. THEOCARIS, *J. Appl. Mech.* **37** ASME Vol. 92, Series E (1970) 409.
34. *Idem,* "Development in Stress Analysis", Vol. 1, edited by G. Holister (Applied Science Publishers, London, 1978) Ch. 2, p. 27.

Received 18 April
and accepted 29 September 1989